

Local convective heat transfer coefficient and friction factor of CuO/water nanofluid in a microchannel heat sink

A. R. Chabi¹ · S. Zarrinabadi¹ · S. M. Peyghambarzadeh¹ · S. H. Hashemabadi² · M. Salimi¹

Received: 23 January 2016 / Accepted: 6 June 2016 / Published online: 9 June 2016
© Springer-Verlag Berlin Heidelberg 2016

Abstract Forced convective heat transfer in a microchannel heat sink (MCHS) using CuO/water nanofluids with 0.1 and 0.2 vol% as coolant was investigated. The experiments were focused on the heat transfer enhancement in the channel entrance region at $Re < 1800$. Hydraulic performance of the MCHS was also estimated by measuring friction factor and pressure drop. Results showed that higher convective heat transfer coefficient was obtained at the microchannel entrance. Maximum enhancement of the average heat transfer coefficient compared with deionized water was about 40 % for 0.2 vol% nanofluid at $Re = 1150$. Enhancement of the convective heat transfer coefficient of nanofluid decreased with further increasing of Reynolds number.

List of symbols

A	Surface area (m ²)
C _p	Specific heat (J/kg K)
D _h	Hydraulic diameter (m)
f	Fanning friction factor
h	Heat transfer coefficient (W/m ² K)
H _{ch}	Height of microchannel (μm)
H _{tc}	Distance from thermocouple to the base of microchannel (mm)
K	Thermal conductivity (W/m K)
L _{ch}	Microchannel length (mm)
\dot{m}	Mass flow rate (g/s)

Nu	Nusselt number
n	solid particle shape factor
N	Number of microchannel
Pr	Prandtl number
Δp_{net}	Net pressure drop along microchannels (bar)
$\Delta p_{measured}$	Total pressure drop (bar)
$\Delta p_{c1}, \Delta p_{c2}$	Contraction pressure loss (bar)
$\Delta p_{e1}, \Delta p_{e2}$	Expansion pressure loss (bar)
q _f	Heat transfer rate remove by fluid (W)
q _{conv}	Heat flux through heat sink base area by convection mechanism (W/m ²)
Re	Reynolds number
T	Temperature (°C)
\bar{u}	Average fluid velocity (m/s)
u _{in}	Fluid inlet velocity (m/s)
u _{out}	Fluid outlet velocity (m/s)
w _{ch}	Microchannel width (μm)
w _{fin}	Fin width (μm)
x	Axial distance (mm)

Greeks

η	Fin efficiency
μ	Viscosity
ρ	Density
φ	Volumetric fraction of nanoparticles

Subscripts

ave	Average
b	Bulk
bf	Base fluid
ch	Microchannel
fin	Fin
in	Inlet
nf	Nanofluid
out	Outlet

✉ S. M. Peyghambarzadeh
peyghambarzadeh@gmail.com

¹ Department of Chemical Engineering, Mahshahr branch, Islamic Azad University, Mahshahr, Iran

² CFD Research Laboratory, School of Chemical Engineering, Iran University of Science and Technology, Narmak, Tehran 16846, Iran

p	Solid particles
s	Solid metal for heat sink
w	Wall
x	Local condition

1 Introduction

Technology progress in the fields such as: electronic industries, high power engines and optical devices that produce high heat flux is in a way that conventional methods are not able to remove the heat generated by these devices. These devices need to advance cooling methods. There are two ways to improve the cooling processes. The first technique is design of new cooling device with smaller channel dimensions that causes enhanced convective heat transfer coefficient due to increased fluid velocity [1, 2]. In this regards, the use of microchannels as a cooling device for dissipating heat from silicon integrated circuit was first proposed by Tuckerman and Pease [3]. Two important goals in the electronics cooling are the reduction of maximum temperature of the device, and minimization of temperature gradients on the surface that can be achieved by the use of MCHS [4]. The second way of enhancing cooling process is improving the heat transfer properties of the coolant fluids [5–9]. Since the thermal conductivity of metallic solids is much higher than the fluids, use of suspended millimeter or micrometer sized metallic solid particles in the fluid is expected to enhance the thermal conductivity of the base fluid [10]. To overcome the problems such as: abrasion, particles sedimentation, clogging, and finally additional pressure drop along the channel that occurs due to the large size of particles, the novel concept of nanofluid was first introduced by Choi and Eastman [11]. They carried out several experiments to suspend various metal and metal oxide nanoparticles in different base fluids [5, 12–15].

Due to the importance of MCHS in the cooling processes, numerical and experimental studies of thermal and flow behavior in the MCHS are increasing. Mirzaei and Dehghan [16] numerically investigated flow and heat transfer of water/ Al_2O_3 nanofluid in a microchannel with variable property approach. Chein and Huang [17] experimentally investigated forced convective heat transfer performance of 0.3–2 vol% Cu/water nanofluids in a silicon microchannel with $100 \times 300 \mu\text{m}$ dimensions. Their results showed that Nusselt number increases with increase of Reynolds number and nanofluid concentration. In their experiments, maximum reduction of the thermal resistance was 15 % in comparison with pure water which was occurred at 2 vol% of nanofluid. Sivakumar et al. [18] experimentally investigated comparison of heat transfer performance of Al_2O_3 /water and CuO/water nanofluids in a serpentine shape microchannel heat sink.

Nguyen et al. [19] investigated enhancement of convective heat transfer of Al_2O_3 /water nanofluid in the electronics cooling systems. Their experimental results showed that the convective heat transfer coefficient of nanofluid in the turbulent flow regime at 6.8 vol% concentration was 40 % higher than that of pure water. They also experimentally evaluated the effect of nanoparticle size on the heat transfer coefficient using 36 and 47 nm Al_2O_3 nanoparticles. It was concluded that the heat transfer coefficient decreases with increasing the particle size. Zhingang et al. [20] experimentally studied single phase heat transfer of deionized water in the quartz grass microtubes with 45–141 μm inner diameters. The experiments were conducted in the range of Reynolds number from 100 up to 3000. The experimental Nusselt numbers were obtained at lower Reynolds number in the laminar regime were less than the values predicted by classical correlations. They observed that the experimental data sharply increased with increasing the Reynolds number, and the experimental Nusselt numbers were higher than those predicted by transitional classical correlations.

Ho et al. [21] experimentally investigated the cooling performance of a rectangular MCHS with $800 \times 283 \mu\text{m}$ dimensions using Al_2O_3 /water nanofluid as the working fluid at $226 < \text{Re} < 1676$ and constant wall temperature condition. Their results showed that the average Nusselt number for 1 vol% nanofluid increased about 53 % at $\text{Re} = 1641$. They also found that for lower Reynolds numbers, further increasing of the nanofluid concentration from 1 to 2 vol% didn't have appreciable effect on the heat transfer enhancement due to agglomeration of the nanoparticles. The similar effects of nanoparticle deposition were also reported by Chein and Hung [22] and Lee and Mudawar [23].

Agwu Nnanna [24] experimentally evaluated thermo-hydraulic behavior of rectangular microchannel heat exchanger with 87 μm channel width and 0.17 mm hydraulic diameter. They found that there is an optimum Reynolds number to have maximum heat transfer performance. This optimum Reynolds number led to minimum junction temperature. The optimum Reynolds number is depending on the geometrical properties of the microchannel.

Byrne et al. [25] experimentally studied the effect of cetyltrimethyl ammonium bromide (CTAB) surfactant as a dispersant on the heat transfer at different concentrations of CuO/water nanofluids in a parallel microchannel flow configuration using dynamic light scattering technique. They observed that 0.1 vol% of nanofluid negatively affects the heat transfer coefficient unless an appropriate surfactant is used. Selvakumar and Suresh [26] measured the convective heat transfer coefficient of CuO/water nanofluid in an electronic heat sink. They found that the convective heat transfer coefficient of nanofluid increased with increasing flow rate and nanofluid concentration in

the turbulent flow. Maximum enhancement of about 29 % was occurred at 2 vol% of nanoparticles in the base fluid. They also proposed a correlation for Nusselt number at $14,500 < Re < 44,000$ in the microchannel.

Regarding the short channel length in the microchannel heat sink, the effect of channel entrance length is considerable in comparison with the channel length. In this paper, local heat transfer coefficient at the entrance region was measured using CuO/water nanofluid as the working fluid. Similar experimental works were less performed before due to the some restrictions in the experimental setup fabrication. Since the heat transfer coefficient was measured at the channel entrance, it is possible to compare the effect of flow condition and nanoparticle concentration at this region with those in the remaining section of the microchannel. Really, the novelty of this paper which distinguishes it from the previous researches includes:

- The heat transfer coefficient at the channel entrance was compared with that in the region far from the entrance (fully developed region).
- The effect of operating conditions on the heat transfer coefficient at the entrance region was analyzed and the optimum operating conditions was obtained.

2 Experimental

2.1 Setup and procedure

A schematic of the experimental flow loop used in this investigation is shown in Fig. 1. This setup mainly consisted of liquid reservoir, gear pump, MCHS, cartridge

heaters, pressure transmitter and constant temperature bath. The working fluid at 24.5 °C was pumped by the variable rotation speed gear pump (Gear pump, model: CS-0720B-CSE Co., Korea made) through the MCHS and continuously circulated in the closed-loop. The heat generated by the heaters in the MCHS was absorbed by the working fluid. The outlet liquid passed through the constant temperature bath to have constant liquid inlet temperature. As shown in Fig. 1, liquid temperature was adjusted by a bypass line and a needle valve at various flow rates. The mass flow rate was directly measured by an electronic balance and a stopwatch at various times after beginning of the experiment. The test section shown in Fig. 2 includes the MCHS and housing. The housing was made from Plexiglas and for the purpose of sealing, the Room Temperature Vulcanizing (RTV) silicon rubber was used between test block and housing.

The test block was fabricated from an alloy of oxygen-free copper–beryllium (Cu-Be) with total dimensions of $50 \times 14 \times 50$ mm in length, width and, height, respectively. As shown in Fig. 3, 17 rectangular channels with 400 μm width and 560 μm height were machined on the top surface of the test block by wire electrical discharge.

To measure the temperature along a microchannel, four K-type thermocouples with 1 mm diameter were installed at the distance of 5 mm beneath the bottom surface of the microchannels in the block. Details of thermocouples location in the block are shown in Fig. 4 and listed in Table 1. To measure the fluid temperature and pressure at the inlet and outlet of the microchannels, two K-type thermocouples and pressure transmitters (Trafag, model: 8472, Switzerland) were located at the inlet and outlet pendulums which are demonstrated in Fig. 5. To provide heating, five

Fig. 1 Schematic of the MCHS experimental setup

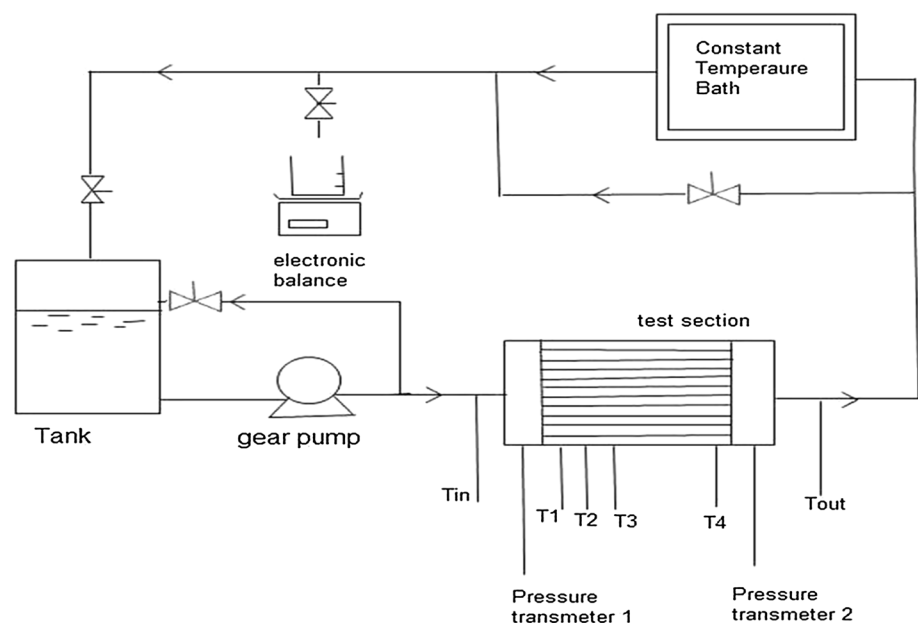


Fig. 2 Test section block

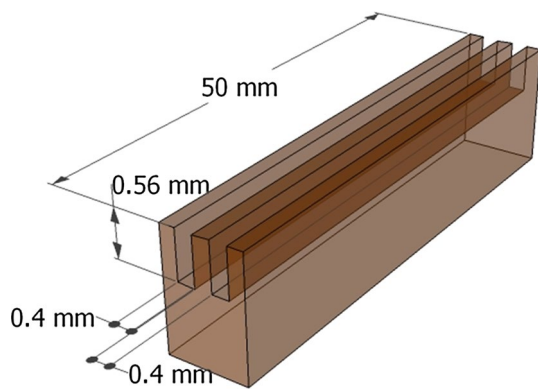
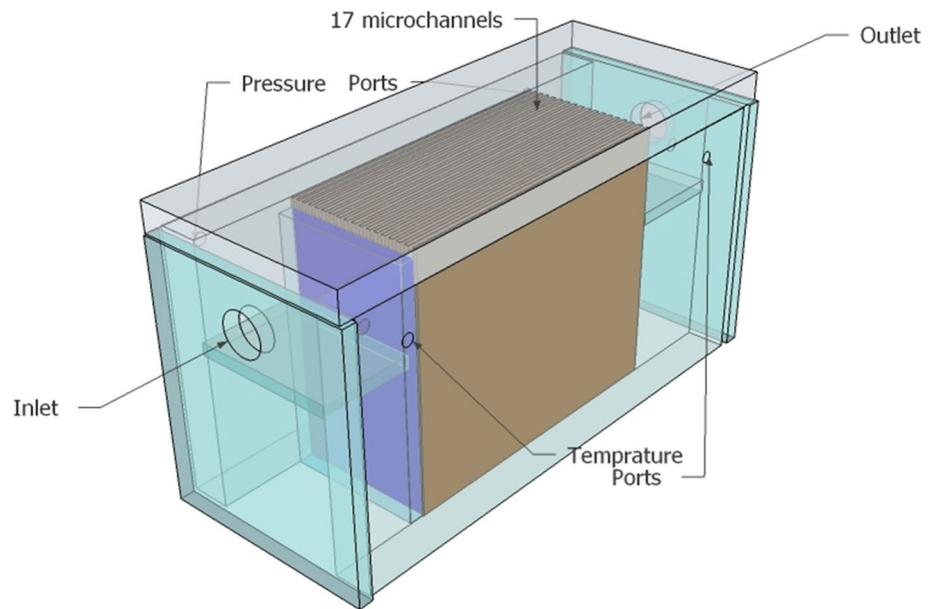


Fig. 3 Dimensions of the microchannels

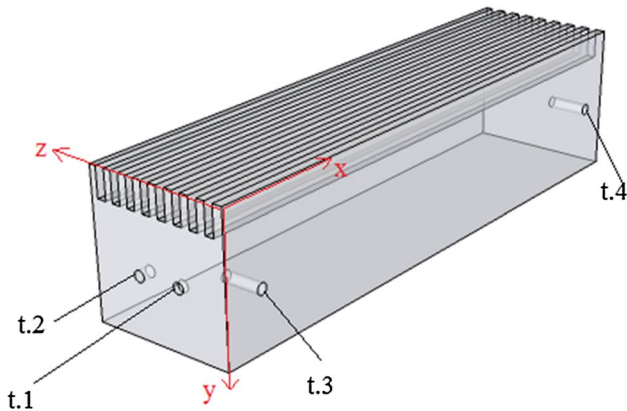


Fig. 4 Thermocouple locations in the block

Table 1 Details of thermocouple locations in the block (all dimensions are in mm)

Direction	t.1	t.2	t.3	t.4
x	0.8 (deep)	1.5 (deep)	3	47
y	5 + 0.56	5 + 0.56	5 + 0.56	5 + 0.56
z	5	9	5 (deep)	5 (deep)

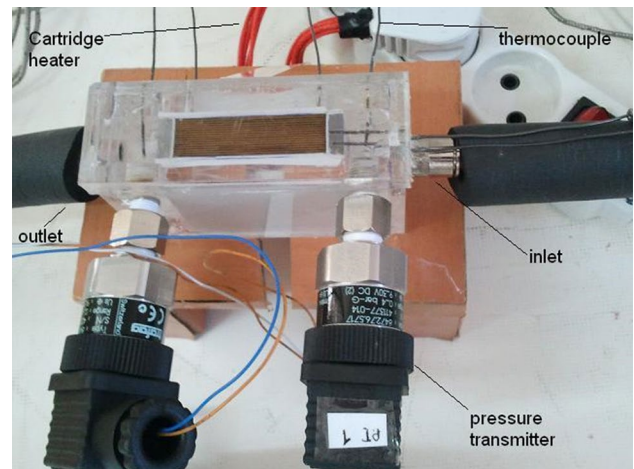


Fig. 5 Actual view of test block

cartridge heaters with diameter of 6 mm and total maximum power of 750 W werelocated into the bottom of block as shown in Fig. 6. The input power was adjusted by a DC power supply unit.

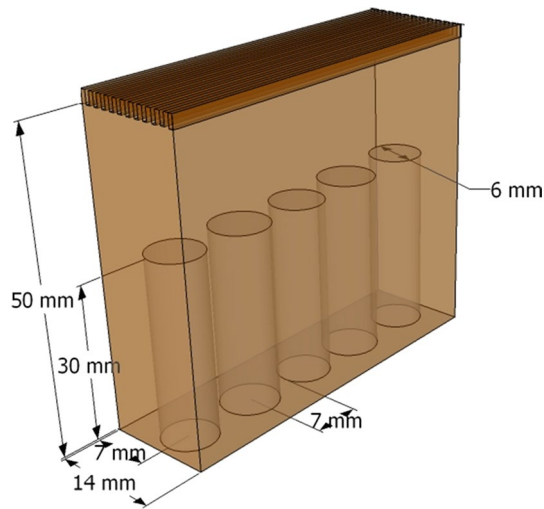


Fig. 6 Schematic of arrangement of the cartridge heaters in the test block

Table 2 The uncertainty of measured parameters

Parameter	Value	Max. uncertainty (%)
Re	600–1800	6.1
h (W/m ² K)	6900–17,200	23.2
Nu	5.2–13	23.5
f	0.01–0.03	6.7

2.2 Uncertainty analysis

The experimental uncertainties in a microchannel can be quite large due to very small dimensions of the test section and very high heat transfer coefficient which causes small temperature differences between the surface and the fluid. Uncertainty analysis in the present work was carried out according to the method described by Moffat [27]. The experimental uncertainty for temperature was estimated to be ± 0.3 °C. The uncertainties of the deduced experimental results are summarized in Table 2.

3 Nanofluids preparation and properties

To prepare CuO/water nanofluid, almost spherical copper oxide nanoparticles (US Research Nanomaterials, Inc., USA) with 40 nm average particle size and 99 % purity were dispersed in deionized water as base fluid. In this study, the nanofluid was stabilized without use of any surfactant to avoid any probable complication. Since pH of nanofluid is an important parameter to prepare stable nanofluid suspension, stabilization at different pH values was measured by the photography sedimentation method. It is

found that nanofluid at pH = 3 shows better stability for a long time. Two volumetric percent of CuO/water nanofluid ($\varphi = 0.1$ and 0.2) were prepared by mixing appropriate quantities of copper oxide nanoparticles in deionized water by using an ultrasonic vibration bath (Bandelin, model:dk, Germany) for 3 h. Very small amount of precipitation was observed after 8 h. The thermophysical properties of CuO/water nanofluid were calculated based on the mean fluid temperature (i.e. average of the fluid temperature at the inlet and outlet) by the following correlations:

Density [28]:

$$\rho_{nf} = (1 - \varphi)\rho_{bf} + \varphi\rho_p \quad (1)$$

Specific heat capacity [29]:

$$C_{p,nf} = \frac{(1 - \varphi)\rho_{bf}C_{p,bf} + \varphi\rho_pC_{p,p}}{\rho_{nf}} \quad (2)$$

For estimating the viscosity of liquid suspension, the following equation was first proposed by Einstein [30]:

$$\mu_{nf} = \mu_{bf}(1 + 2.5\varphi) \quad (3)$$

Equation (3) is used only for dilute suspension ($\varphi \leq 0.02$ vol%). Since, the volumetric percent of the nanofluid in the present work is more than 0.02 %, the viscosity of nanofluid was calculated using Einstein–Batechelor equation [31]:

$$\mu_{nf} = \mu_{bf}(1 + 2.5\varphi + 6.2\varphi^2 + \dots) \quad (4)$$

According to the experimental study performed by Nguyen et al. [32] for the measurement of the viscosity of nanofluid, the viscosity of CuO/water nanofluid at low volume fraction ($\varphi < 1$ vol%) is in good agreement with Einstein–Batechelor equation.

Hamilton and Crosser correlation [33] was also used for determination of effective thermal conductivity of nanofluid as follows:

$$k_{nf} = \frac{k_p + (n - 1)k_{bf} - \varphi(n - 1)(k_{bf} - k_p)}{k_p + (n - 1)k_{bf} + \varphi(k_{bf} - k_p)}k_{bf} \quad (5)$$

where n is the empirical shape factor which is equal to 3 for the spherical particles. In the above equations, subscribes bf, p and nf refer to the base fluid, particle, and nanofluid, respectively.

4 Data reduction

In this investigation, variation of heat transfer coefficient of CuO/water nanofluid along the microchannel was measured experimentally. All experiments were carried out at Reynolds number range between 600 and 1800 and two volumetric percent ($\varphi = 0.1$ and 0.2). In the specific flow rate,

the temperatures and pressure drop along the microchannel were reached to steady state condition after approximately 40 min. The heat absorbed by the coolant can be determined as follows:

$$q_f = \dot{m}C_p(T_{out} - T_{in}) \tag{6}$$

Since the experiments were performed at the constant heat flux condition, the amount of absorbed heat by the coolant is about 130 W. The heat loss due to conduction losses from sides of copper block and insulations were calculated about 18 % of the heat input.

The base wall temperature of the microchannels (T_w) was calculated from Eq. (7) by assuming one dimensional heat conduction. It was calculated from the readings from thermocouples located at the 5 mm underneath the base surface of the microchannels [21]:

$$T_{w,x} = T_{tc,x} - \frac{q_f \times H_{tc}}{N \cdot L_{ch} \cdot k_s \cdot (w_{ch} + w_{fin})} \tag{7}$$

where H_{tc} is distance of thermocouple location from the base surface of the microchannel and k_s is the thermal conductivity of copper block and N is number of channels.

The local fluid bulk temperatures along the microchannels were calculated as follows:

$$T_{b,x} = T_{in} + \frac{q''_{conv} \times (2\eta_{fin}H_{ch} + w_{ch})x \times N}{\dot{m}c_p} \tag{8}$$

The local convective heat transfer coefficient can be derived as follows [23]:

$$h_x = \frac{q''_{conv}}{T_{w,x} - T_{b,x}} = \frac{q_f}{(2\eta_{fin}H_{ch} + w_{ch})L_{ch} \cdot N (T_{w,x} - T_{b,x})} \tag{9}$$

where x is the distance from channel inlet and η_{fin} denotes the fin efficiency calculated from the following equation [34]:

$$\eta_{fin} = \frac{\tanh(mH_{ch})}{mH_{ch}} \tag{10}$$

where m is fin parameter and determined by:

$$m = \sqrt{2 \frac{h_x}{K_s w_{fin}}} \tag{11}$$

The average convective heat transfer coefficient and Nusselt number can be calculated as:

$$h_{avg.} = \frac{\int h_x dA}{A} \tag{12}$$

$$Nu = \frac{h_{avg.} D_h}{k_f} \tag{13}$$

where k_f is fluid thermal conductivity.

The Reynolds number was calculated as follow:

$$Re = \rho u D_h / \mu \tag{14}$$

Since the pressure transmitters were inserted in the inlet and outlet manifolds, measured pressure drop consisted of net pressure drop along the microchannels (ΔP_{net}) and four extra pressure losses due to abrupt contractions and expansions; two inlet contraction pressure losses from deep plenum to shallow plenum (ΔP_{c1}), and from shallow plenum to the microchannels inlet (ΔP_{c2}), two outlet expansion pressure recoveries from the microchannels outlet to shallow plenum (ΔP_{e2}), and from shallow plenum to deep plenum (ΔP_{e1}). The net pressure drop can be calculated by the method described by Qu and Mudawar [35].

$$\Delta P_{net} = \Delta P_{measured} - (\Delta P_{c1} + \Delta P_{c2} + \Delta P_{e1} + \Delta P_{e2}) \tag{15}$$

$$\Delta P_{c1} = \frac{1}{2} \rho_{nf} (u_{p2,in}^2 - u_{p1,in}^2) + \frac{K_{c1}}{2} \rho_{nf} u_{p2,in}^2 \tag{16}$$

$$\Delta P_{c2} = \frac{1}{2} \rho_{nf} (u_{in}^2 - u_{p2,in}^2) + \frac{K_{c2}}{2} \rho_{nf} u_{in}^2 \tag{17}$$

$$\Delta P_{e2} = \frac{1}{2} \rho_{nf} (u_{p2,out}^2 - u_{out}^2) + \frac{K_{e2}}{2} \rho_{nf} u_{out}^2 \tag{18}$$

$$\Delta P_{e1} = \frac{1}{2} \rho_{nf} (u_{p1,out}^2 - u_{p2,out}^2) + \frac{K_{e1}}{2} \rho_{nf} u_{p2,out}^2 \tag{19}$$

where subscripts p1 and p2 denote the deep plenum and shallow plenum, respectively. K_c and K_e are the loss coefficient for the abrupt contractions and the abrupt expansions, respectively. The values of K_c and K_e were obtained from [36].

5 Results and discussion

5.1 Local wall temperature

The local wall temperatures of the microchannels were measured by four thermocouples located along the microchannels length as previously shown in Fig. 4. Figure 7 shows the axial variation of the wall temperature of the microchannels. It is clear from Fig. 7 that the microchannel wall temperature decreases with increasing Reynolds number due to increased flow turbulence. It also decreases with increasing nanofluid concentration due to improved heat transfer coefficient of fluid. There are four possible mechanisms for heat transfer enhancement with nanofluids which proposed by Keblinski et al. [37]: Brownian motion,

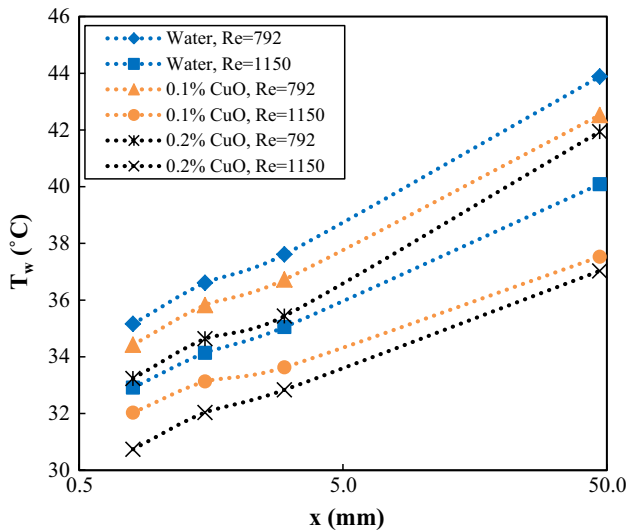


Fig. 7 Axial wall temperature along the microchannel length for different flow rates and nanofluid concentrations

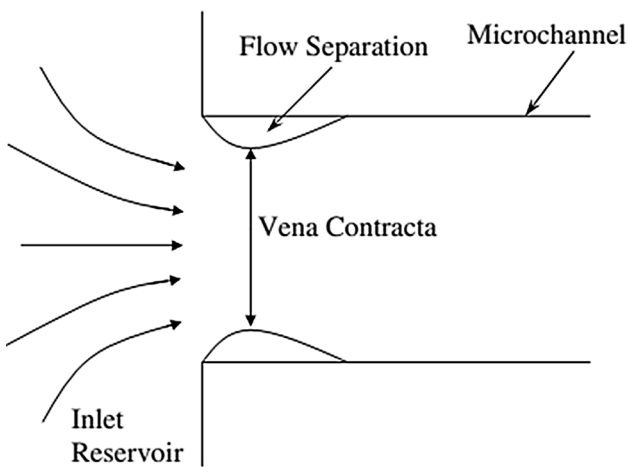


Fig. 8 Vena contracta effect at the entrance region of the microchannel

ballistic phonon transport, layering at the liquid/particle interface and nanoparticle clustering.

5.2 Convective heat transfer coefficient

According to the measured microchannel wall temperatures, fluid bulk temperature and heat absorbed by the fluid, the local convective heat transfer coefficient was calculated from Eq. (9). Figure 8 illustrates the variation of local convective heat transfer coefficient of deionized water along the microchannel length. According to this figure, at the constant Re, the heat transfer coefficient at the channel entrance is higher than that in the other locations along the microchannel. The heat transfer coefficient decreases along

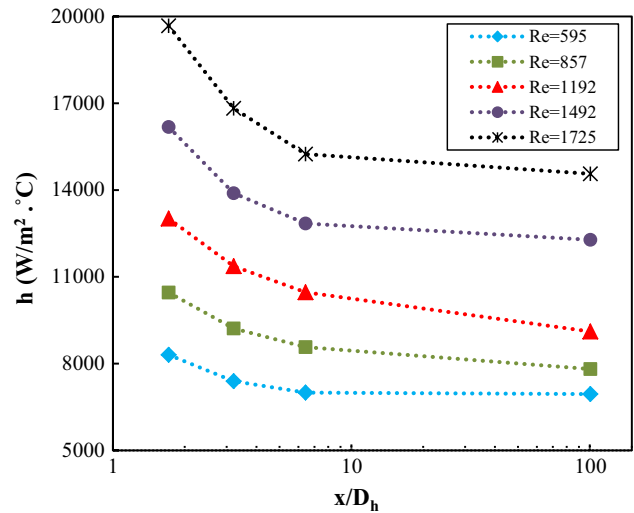


Fig. 9 Variation of local convective heat transfer coefficient of base fluid (water) along the microchannel length

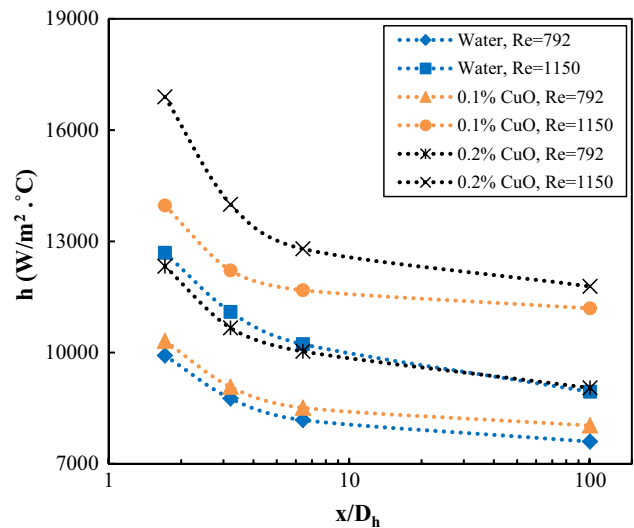


Fig. 10 Variation of local convective heat transfer coefficient of nanofluid and base fluid at different Re and nanofluid concentrations along the microchannel length

the microchannel due to increase of thermal boundary layer thickness in the developing region. Another important reason for increased heat transfer coefficient at the entrance region is due to increase of flow disturbance at the channel inlet which itself caused by sudden flow contraction. Figure 8 shows the schematic corner of sharp edged of channel inlet that produces flow separation effect and vena contracta effect. The vena contracta size extended with increases Reynolds number [38]. Since the entrance region effect depends on Reynolds number [38, 39], increase in the convective heat transfer coefficient at the entrance region becomes more pronounced with increasing Reynolds

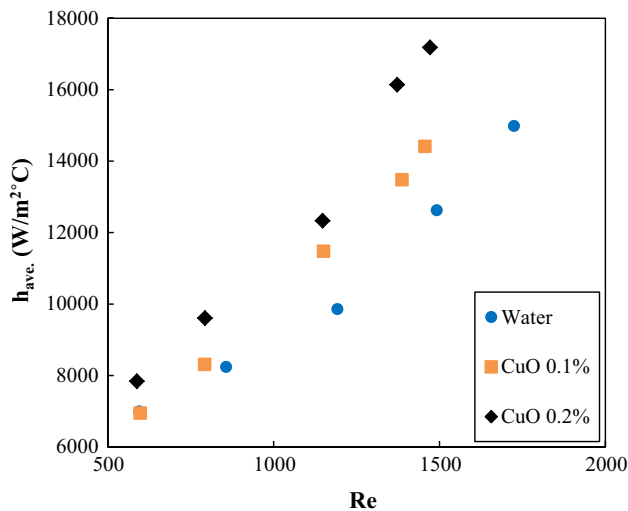


Fig. 11 Average heat transfer coefficient versus Re for water and CuO/water nanofluids

number as shown in Fig. 9. The similar results were also reported in [40]. Variation of local convective heat transfer coefficient of water, 0.1 and 0.2 vol% of CuO/water nanofluids at two Reynolds numbers along the microchannel are shown in Fig. 10. As shown in this figure, the convective heat transfer coefficient along the microchannel decreases; this is due to the flow developing and also increase of the boundary layer thickness. Maximum enhancement of the local convective heat transfer coefficient compared with the base fluid was about 50 % for 0.2 vol% of the nanofluid which was occurred at $Re = 1450$ and $x = 0.8$ mm.

The entrance region effect often is not considered at the conventional channels due to its short length in comparison with the channel length. Calculating the average convective heat transfer coefficient of microchannels without considering high value of heat transfer coefficient at the entrance region, may cause considerable error in the averaging. Figure 11 depicts the average heat transfer coefficient of water and nanofluids which was calculated from Eq. (12). The convective heat transfer coefficient increased with increasing Reynolds number and nanofluid concentration. Maximum enhancement of the average heat transfer coefficient for 0.1 and 0.2 vol% of CuO/water nanofluids were 18 and 40 % respectively, compared with deionized water which were occurred at $Re = 1150$. Further increase in the fluid flow rate (or Reynold number) caused lower increase in the heat transfer coefficient. It might be happened due to deposition of nanoparticles at higher Reynolds number as reported by Ho et al. [21], and Chein and Chuang [22]. Deposition of nanoparticles is a complicated process which comprises interactions between particles and between wall and particles. Such interactions depend on shape, size, electrochemical and thermophysical properties of particles,

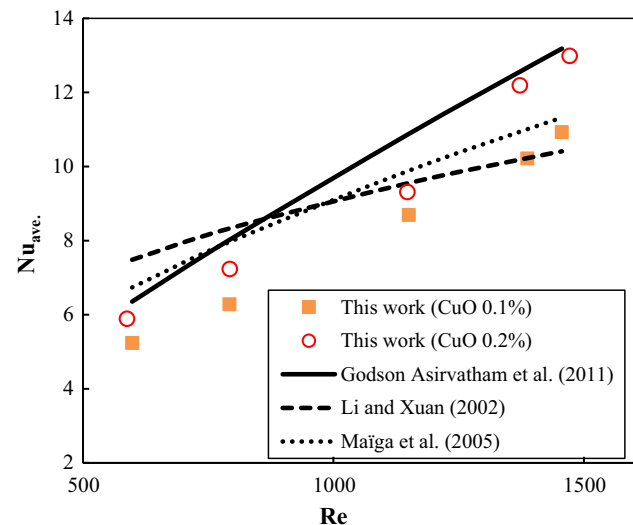


Fig. 12 Experimental average Nu number and comparison with other correlations for 0.1 and 0.2 vol% of CuO/water nanofluid

base fluid, as well as bulk and wall temperatures [41]. Therefore, answering to most of questions about nanoparticle deposition requires the knowledge and understanding of these interactions which is beyond the scope of this paper.

Figure 12 compares the experimental Nusselt number with the prediction of correlations suggested by Godson Asirvatham et al. [42], Li and Xuan [43] and Maïga et al. [44] for 0.1 and 0.2 vol% CuO/water nanofluids. These correlations are presented in Table 3. Nusselt number of nanofluids depends on many factors such as: thermal conductivity, heat capacity of nanoparticle and base fluid, volume fraction of nanoparticles in base fluid, particle size and shape, flow regime and viscosity of nanofluid [45]. Despite of multiplicity of the factors affecting Nusselt number, the experimental Nusselt number of this work seems to be in good agreement with the correlations that mentioned above, particularly with the correlation suggested by Godson Asirvatham et al. [42]. As can be seen in Table 4, the absolute average errors of the correlation suggested by Godson Asirvatham et al. [42] in the prediction of Nusselt number for 0.1 and 0.2 vol% CuO/water nanofluid are about 8.5 and 7.6 %, respectively.

5.3 Pressure drop and friction factor

Some of the previous studies showed that use of nanofluids as coolant in microchannels causes higher pressure drop in comparison with the base fluid [21–23, 46–50]. Larger pressure drop occurs firstly due to larger viscosity of nanofluids compared with the base fluid (Eq. 4). Secondly, particles deposition increases wall roughness and consequently, causes smaller cross sectional flow area. To ensure the

Table 3 Empirical forced convection heat transfer correlations

Author	Correlation	Relevant information
Li and Xuan [43]	$Nu = 0.4328(1.0 + 11.285\varphi^{0.754}Pe_p^{0.218})Re_{nf}^{0.333}Pr_{nf}^{0.4}$	Cu/water 0.3 < ϕ < 2 vol%, Re \geq 800
Maiga et al. [44]	$Nu = 0.86Re^{0.55}Pr^{0.5}$	Al ₂ O ₃ /water, Al ₂ O ₃ /EG $\phi \leq 10$ vol%, Re ≤ 1000
Godson Asirvatham et al. [42]	$Nu = 0.023Re^{0.8}Pr^{0.3} + (0.617\varphi - 0.135)Re^{(0.445\varphi - 0.37)}Pr^{(1.081\varphi - 1.305)}$	Silver/Water 0.3 < ϕ < 0.9 vol%, 900 \leq Re \leq 12,000

Table 4 Absolute average errors in the prediction of Nu number using the available correlations in comparison with the present experimental data

CuO/water nano-fluids (%)	Maiga et al. [44] (%)	Godson Asirvatham et al. [42] (%)	Li and Xuan [43] (%)
$\varphi = 0.1$	16.10	8.50	18.10
$\varphi = 0.2$	10.30	7.60	16.90

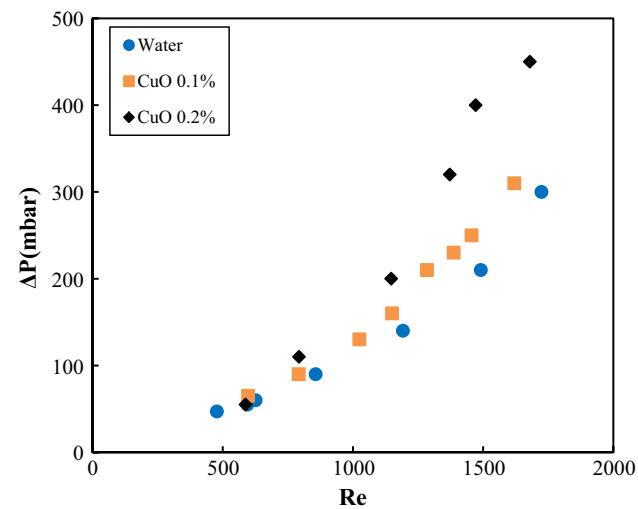


Fig. 13 Variation of net pressure drop in the microchannels versus Reynolds number for water and CuO/water nanofluids

benefit of nanofluid, the pressure drop along the micro-channel experimentally measured by two pressure transmitters installed at the inlet and outlet plenums of the module. Figure 13 shows the variation of net pressure drop against Reynolds number. Net pressure drop was determined according to the method described by Qu and Mudawar [35], eliminating pressure losses at the inlet contractions and outlet expansions (Eq. 15). The microchannel friction factor is obtained from Eq. (20) and shown in Fig. 14 for deionized water and CuO/water nanofluids. The experimental friction factor for Al₂O₃/water nanofluid at 2 vol% reported by Ho et al. [21] was also shown in Fig. 14 for

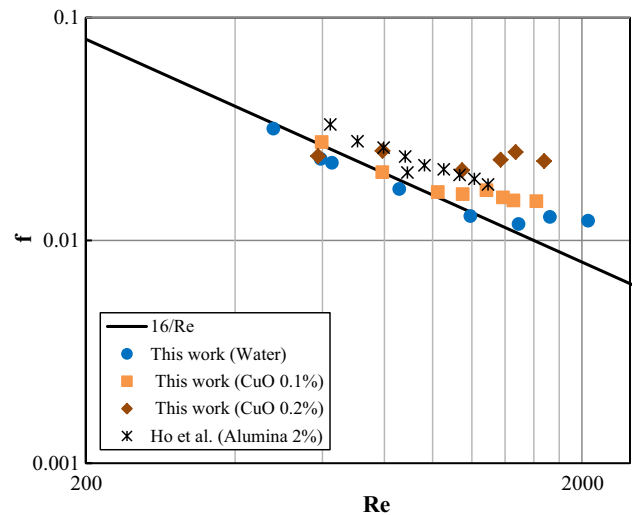


Fig. 14 Variation of friction factor versus Reynolds number for the base fluid and nanofluids

comparison. According to Fig. 14, the experimental data related to the friction factor are in good agreement with well-known relation for laminar flow regime, $f = 16/Re$.

$$fRe = \frac{D_h^2}{2\mu\bar{u}} \left(\frac{\Delta P}{\Delta x} \right). \tag{20}$$

6 Conclusion

In the present study, the enhancement of convective heat transfer coefficient of CuO/water nanofluids at 0.1 and 0.2 vol% in a rectangular MCHS was experimentally investigated. This work specially focused on the local convective heat transfer coefficient at the entrance region of the microchannel. Experimental results showed that convective heat transfer coefficient enhances with increasing Reynolds number and nanofluid concentration. Further increase in the fluid flow rate and nanofluid concentration deteriorates the heat transfer coefficient enhancement. It is due to rapid formation of sediment and nanofluid instability. The maximum local heat transfer coefficient was observed at the channel entrance due to the entrance region effect and

minimum boundary layer thickness. The results showed that the entrance region effect depends on the Reynolds number, and higher Reynolds number causes higher entrance region effect. Considerable enhancement of the average heat transfer coefficient was obtained compared with deionized water. For the cases of 0.1 and 0.2 vol% of CuO/water nanofluids, 18 and 40 % enhancements were respectively obtained.

References

- Han Z (2008) Nanofluids with enhanced thermal transport properties. Ph.D. thesis, University of Maryland at College Park, Maryland
- Kebllinski P, Eastman JA, Cahill DG (2005) Nanofluids for thermal transport. *Mater Today* 8(6):36–44
- Tuckerman DB, Pease R (1981) High-performance heat sinking for VLSI. *Electron Device Lett IEEE* 2(5):126–129
- Garimella SV, Sobhan C (2003) Transport in microchannels—a critical review. *Annu Rev Heat Transf* 13:1–50
- Eastman JA, Phillpot S, Choi S, Kebllinski P (2004) Thermal transport in nanofluids. *Annu Rev Mater Res* 34:219–246
- Mohammed HA, Bhaskaran G, Shuaib NH, Saidur R (2011) Heat transfer and fluid flow characteristics in microchannels heat exchanger using nanofluids: a review. *Renew Sustain Energy Rev* 15(3):1502–1512
- Peighambarzadeh S, Hashemabadi S, Jamnani MS, Hoseini S (2011) Improving the cooling performance of automobile radiator with Al₂O₃/water nanofluid. *Appl Therm Eng* 31(10):1833–1838
- Peighambarzadeh SM, Hashemabadi SH, Naraki M, Vermahmoudi Y (2013) Experimental study of overall heat transfer coefficient in the application of dilute nanofluids in the car radiator. *Appl Therm Eng* 52(1):8–16. doi:10.1016/j.applthermaleng.2012.11.013
- Vakili M, Mohebbi A, Hashemipour H (2013) Experimental study on convective heat transfer of TiO₂ nanofluids. *Heat Mass Transf* 49(8):1159–1165
- Fotukian S, Nasr Esfahany M (2010) Experimental study of turbulent convective heat transfer and pressure drop of dilute CuO/water nanofluid inside a circular tube. *Int Commun Heat Mass Transf* 37(2):214–219
- Choi SUS, Eastman J (1995) Enhancing thermal conductivity of fluids with nanoparticles. Argonne National Lab, Lemont, IL
- Choi SUS (1998) Nanofluid technology: current status and future research. Argonne National Lab, Lemont, IL
- Eastman J, Choi U, Li S, Soyez G, Thompson L, DiMelfi R (1999) Novel thermal properties of nanostructured materials. *J Metastable Nanocryst Mater* 2:629–634
- Choi S, Zhang Z, Yu W, Lockwood F, Grulke E (2001) Anomalous thermal conductivity enhancement in nanotube suspensions. *Appl Phys Lett* 79(14):2252–2254
- Eastman J, Choi S, Li S, Yu W, Thompson L (2001) Anomalous increased effective thermal conductivities of ethylene glycol-based nanofluids containing copper nanoparticles. *Appl Phys Lett* 78(6):718–720
- Mirzaei M, Dehghan M (2013) Investigation of flow and heat transfer of nanofluid in microchannel with variable property approach. *Heat Mass Transf* 49(12):1803–1811
- Chein R, Huang G (2005) Analysis of microchannel heat sink performance using nanofluids. *Appl Therm Eng* 25(17):3104–3114
- Sivakumar A, Alagumurthi N, Senthilvelan T (2015) Experimental investigation of forced convective heat transfer performance in nanofluids of Al₂O₃/water and CuO/water in a serpentine shaped micro channel heat sink. *Heat Mass Transf* 1–10. doi:10.1007/s00231-015-1649-5
- Nguyen CT, Roy G, Gauthier C, Galanis N (2007) Heat transfer enhancement using Al₂O₃–water nanofluid for an electronic liquid cooling system. *Appl Therm Eng* 27(8):1501–1506
- Zhigang L, Ning G, Takei M (2007) An experimental investigation of single-phase heat transfer in 0.045 mm to 0.141 mm microtubes. *Nanoscale Microscale Thermophys Eng* 11(3–4):333–349
- Ho CJ, Wei LC, Li ZW (2010) An experimental investigation of forced convective cooling performance of a microchannel heat sink with Al₂O₃/water nanofluid. *Appl Therm Eng* 30:96–103
- Chein R, Chuang J (2007) Experimental microchannel heat sink performance studies using nanofluids. *Int J Therm Sci* 46(1):57–66
- Lee J, Mudawar I (2007) Assessment of the effectiveness of nanofluids for single-phase and two-phase heat transfer in microchannels. *Int J Heat Mass Transf* 50(3):452–463
- Agwu Nnanna A (2010) Thermo-hydraulic behavior of microchannel heat exchanger system. *Exp Heat Transf* 23(2):157–173
- Byrne MD, Hart RA, da Silva AK (2012) Experimental thermal–hydraulic evaluation of CuO nanofluids in microchannels at various concentrations with and without suspension enhancers. *Int J Heat Mass Transf* 55(9–10):2684–2691. doi:10.1016/j.ijheatmasstransfer.2011.12.018
- Selvakumar P, Suresh S (2012) Convective performance of CuO/water nanofluid in an electronic heat sink. *Exp Therm Fluid Sci* 40:57–63. doi:10.1016/j.expthermflusci.2012.01.033
- Moffat RJ (1988) Describing the uncertainties in experimental results. *Exp Therm Fluid Sci* 1(1):3–17
- Wang XQ, Mujumdar AS (2008) A review on nanofluids-part I: theoretical and numerical investigations. *Braz J Chem Eng* 25(4):613–630
- Maxwell JC (1873) A treatise on electricity and magnetism, vol 1. Oxford University Press, Oxford
- Einstein A (1906) A new determination of the molecular dimensions. *Ann Phys* 19:289–306
- Batchelor G (1976) Brownian diffusion of particles with hydrodynamic interaction. *J Fluid Mech* 74(01):1–29
- Nguyen C, Desgranges F, Roy G, Galanis N, Mare T, Boucher S, Angue Mintsa H (2007) Temperature and particle-size dependent viscosity data for water-based nanofluids–hysteresis phenomenon. *Int J Heat Fluid Flow* 28(6):1492–1506
- Hamilton R, Crosser O (1962) Thermal conductivity of heterogeneous two-component systems. *Ind Eng Chem Fundam* 1(3):187–191
- Holman JP (1986) Heat transfer. McGraw-Hill, New York
- Qu W, Mudawar I (2002) Experimental and numerical study of pressure drop and heat transfer in a single-phase micro-channel heat sink. *Int J Heat Mass Transf* 45(12):2549–2565
- Kays W, London A (1984) Compact heat exchangers. McGraw-Hill, New York
- Kebllinski P, Phillpot S, Choi S, Eastman J (2002) Mechanisms of heat flow in suspensions of nano-sized particles (nanofluids). *Int J Heat Mass Transf* 45(4):855–863
- Ahmad T, Hassan I (2010) Experimental analysis of microchannel entrance length characteristics using microparticle image velocimetry. *J Fluids Eng* 132(4):1–13. doi:10.1115/1.4001292
- Gamrat G, Favre-Marinet M, Asendrych D (2005) Conduction and entrance effects on laminar liquid flow and heat transfer in rectangular microchannels. *Int J Heat Mass Transf* 48(14):2943–2954. doi:10.1016/j.ijheatmasstransfer.2004.10.006

40. Jung JY, Oh HS, Kwak HY (2009) Forced convective heat transfer of nanofluids in microchannels. *Int J Heat Mass Transf* 52(1):466–472
41. Israelachvili JN (1992) *Intermolecular and surface forces*. Academic press, New York
42. Godson Asirvatham L, Raja B, Mohan Lal D, Wongwises S (2011) Convective heat transfer of nanofluids with correlations. *Particuology* 9(6):626–631
43. Li Q, Xuan Y (2002) Convective heat transfer and flow characteristics of Cu-water nanofluid. *Sci China Ser E Technol Sci* 45(4):408–416
44. Maïga SEB, Palm SJ, Nguyen CT, Roy G, Galanis N (2005) Heat transfer enhancement by using nanofluids in forced convection flows. *Int J Heat Fluid Flow* 26(4):530–546
45. Xuan Y, Roetzel W (2000) Conceptions for heat transfer correlation of nanofluids. *Int J Heat Mass Transf* 43(19):3701–3707
46. Wu X, Wu H, Cheng P (2009) Pressure drop and heat transfer of $\text{Al}_2\text{O}_3\text{-H}_2\text{O}$ nanofluids through silicon microchannels. *J Micro-mech Microeng* 19(10):105020
47. Azizi Z, Alamdari A, Malayeri MR (2016) Thermal performance and friction factor of a cylindrical microchannel heat sink cooled by Cu-water nanofluid. *Appl Therm Eng* 99:970–978
48. Peyghambarzadeh SM, Hashemabadi SH, Chabi AR, Salimi M (2014) Performance of water based CuO and Al_2O_3 nanofluids in a Cu–Be alloy heat sink with rectangular microchannels. *Energy Convers Manag* 86:28–38
49. Salimi GM, Peyghambarzadeh SM, Hashemabadi SH, Chabi A (2015) Experimental investigation of convective heat transfer of Al_2O_3 /water nanofluid through the micro heat exchanger. *Modares Mech Eng* 15(2):270–280
50. Azizi Z, Alamdari A, Malayeri MR (2015) Convective heat transfer of Cu–water nanofluid in a cylindrical microchannel heat sink. *Energy Convers Manag* 101:515–524